

RESEARCH ACTIVITIES III

Department of Electronic Structure

III-A Photochemical Synthesis of Exotic Organo-Metallic Clusters with Magnetic Properties

We have succeeded to generate cluster molecular magnets of $(\text{Co})_x(\text{CH})_y(\text{CH}_2)_z$. Although information on the structure of the cluster molecules is not enough, *ab initio* molecular orbital calculation of $(\text{Co})_4(\text{CH})_4(\text{CH}_2)_4$ at B3LYP/6-31G level has suggested a deformed cubane type structure that is composed of four cobalt atoms bridged with CH carbon atoms and CH_2 groups coordinate with the cobalt atoms. Photochemical treatment of $\text{C}_5\text{H}_5\text{Co}(\text{CO})_2$ in dichloromethane generated cobaltocene ($\text{C}_5\text{H}_5\text{CoC}_5\text{H}_5$) and $(\text{Co})_x(\text{CH})_y(\text{CH}_2)_z$ with keeping the chemical balance of Co atoms. The latter species became magnets at temperatures lower than 5 K in a matrix of cobaltocene and its derivatives, showing a hysteresis curve characteristic of single molecular magnets: free rotation for the inversion of external magnetic field across zero field and making their cavities wider suited for rotation. Photochemical treatment of $\text{Co}_4(\text{CO})_{12}$ in dichloromethane produced $(\text{CoCHCH}_2)_4$. The black solid product exhibited residual cohesive magnetization with a blocking temperature of 16 K. Electronic structure of these compounds is also very interesting in relation to the origin of ferromagnetism in such cluster molecular magnets.

III-A-1 Photochemical Generation of Cluster Molecular Magnets: $(\text{CoCHCH}_2)_4$

HINO, Kazuyuki¹; KOSUGI, Kentaroh; SEKIYA, Hiroshi¹; HOSOKOSHI, Yuko; INOUE, Katsuya; NISHI, Nobuyuki
(¹*Kyushu Univ.*)

Development of molecular level magnets is one of the recent topics in nanoscience and nanotechnology. In order to make magnetic molecules with high spin quantum numbers, we focus our attention to cobalt atoms composed of 7 electrons in 3d orbitals and 2 electrons in the 4s orbital. A carbonyl compound $\text{Co}_4(\text{CO})_{12}$ was dissolved in dichloromethane solution and high pressure mercury lamp with UV cut-off filter irradiated the solution in a closed glass vessel with a gas exhaust valve. The product solution was mixed with a large amount of anthracene for embedding product molecules in anthracene matrix. The solution was introduced into a new mass spectrometer (see AR2000, III-A-2) through a liquid chromatograph pump and the solute species were deposited as a helical belt on a titanium drum that was rotating and translating in a sample chamber under vacuum. On the opposite side of the drum, after the rotation of 180° , the solute species were photoionized and desorbed by 355 nm laser pulses. Then the ions were introduced to a reflectron mass spectrometer. The mass number of the main product was 344, and assigned to $(\text{CoCHCH}_2)_4$. The solid formed in the reaction vessel was filtrated by using a Millipore filter with a pore size of 0.2 μm . Magnetic properties of the solid photoproducts were measured with a SQUID magnetometer (Quantum Design MPMS-7S).

Figure 1-a shows $\chi_g T$ change of the photoproducts against temperature, where χ_g is mass susceptibility. It is composed of two kinds of magnetic species. One exhibits antiferromagnetic behavior: the $\chi_g T$ value increases with increasing temperature, while the other behaves ferromagnetically at temperatures lower than

30 K. The former component is highly soluble in dichloromethane, whereas the latter is prone to precipitate in the solution. The $\chi_g T$ change of the washed precipitate shows a maximum value of $3.8 \times 10^{-2} \text{ emu g}^{-1} \text{ K}$ at 20 K. Figure 1-b shows magnetization curves upon temperature cooling with or without magnetic field at 10 Oe. The field cooling aligns the molecular magnets along the magnetic field at temperatures lower than the blocking temperature, 16 K, where the zero-field cooling shows maximum magnetization with reducing magnetization at lower temperatures due to random orientation of the magnets. Figure 1-c shows a hysteresis curve of the magnetization. Although both the residual magnetization and the coercive force are small as compared with pure metallic magnets, the hydrogenated carbon-cobalt clusters with 4 cobalt atoms behave as magnets at temperatures lower than 16 K. In order to raise the blocking temperature, we have to increase the number of cobalt atoms up to several tens in the clusters with keeping cubane type frameworks. The origin of generating a high spin angular momentum is expected to the heavy charge transfer from cobalt atoms to carbon atoms on the basis of our molecular orbital calculation and XPS studies.

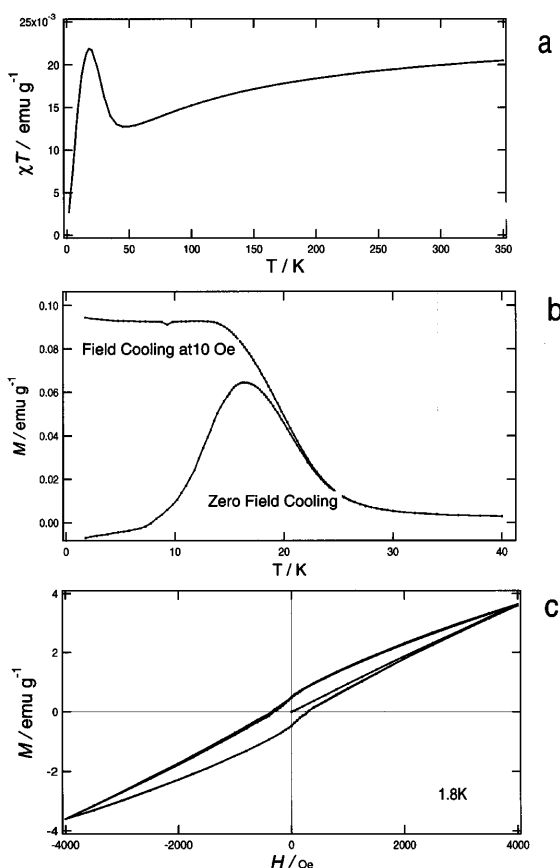


Figure 1. Magnetic properties of photoproducts from $\text{Co}_4(\text{CO})_{12}$ and CH_2Cl_2 ; a: $\chi_g T$ as a function of temperature, b: Magnetization upon field cooling at 10 Oe (upper curve) and on zero field cooling (lower trace), c: hysteresis curve.

III-A-2 Magnetic Behavior of Single Molecular Magnets (Hydrated Carbon-Cobalt Clusters) Isolated in a Glassy Matrix of Cobaltocene and Its Derivatives Generated from Photochemical Reaction of $(\text{C}_5\text{H}_5)\text{Co}(\text{CO})_2$ in Dichloromethane

HINO, Kazuyuki¹; KOSUGI, Kentaroh; SEKIYA, Hiroshi¹; HOSOKOSHI, Yuko; INOUE, Katsuya; NISHI, Nobuyuki
(¹Kyushu Univ.)

Photochemical reaction of $(\text{C}_5\text{H}_5)\text{Co}(\text{CO})_2$ in dichloromethane exhibited release of CO and the following condensation reaction producing cobaltocene, $(\text{C}_5\text{H}_5)\text{Co}(\text{C}_5\text{H}_5)$, and $\text{Co}_x(\text{CH})_y(\text{CH}_2)_z$. The latter cluster products could be generated by the photochemical reaction of solvated cobalt atoms with releasing Cl atoms from reaction intermediates. Secondary reactions also produce bicobaltocene and related compounds, $(\text{C}_5\text{H}_5)\text{Co}(\text{C}_5\text{H}_4-\text{C}_5\text{H}_4)\text{Co}(\text{C}_5\text{H}_5)$, $(\text{C}_5\text{H}_5-\text{C}_5\text{H}_4)\text{Co}(\text{C}_5\text{H}_4-\text{C}_5\text{H}_5)$, $(\text{C}_5\text{H}_5)\text{Co}(\text{C}_5\text{H}_4-\text{C}_5\text{H}_5)$, making the solid products glassy. Very fine particles were observed by a scanning electron microscope as spherical balls of the order of several hundred nm. Although the concentration of the hydrogenated carbon-cobalt clusters, $\text{Co}_x(\text{CH})_y(\text{CH}_2)_z$, is higher in the filtrate solution, the fine particles also contains the clusters as much as approximately 5% of cobaltocene matrices as found by the laser ionization/desorption mass

spectrometry of the solid products.

The $\chi_g T$ change of the fine particles behaved as a superparamagnetic material showing beautifully flat plateau at a level of $0.01 \text{ emu g}^{-1} \text{ K}$ in the temperature range from 50 K to 350 K. At the lower temperatures it increases exhibiting a maximum at 6 K as high as $0.05 \text{ emu g}^{-1} \text{ K}$. The blocking temperature of 6 K was obtained from the ac magnetization measurement. The hysteresis curve is shown in Figure 1-a. One can see the following very interesting features characteristic of single molecular magnets in a matrix composed of bulky molecules: 1; the magnetization loop obtained after several cycles of external field modulation is located much higher than the initial magnetization rise curve, 2; at $0 (\pm 10)$ Oe the magnetization decreases very quickly. These features indicate that the alignment and the rotation of magnetic molecules following the change of the external magnetic field make the space for the magnetic molecules suited for free rotation. The orientational alignment of the spin axes of the magnets became much better when the magnets have experienced rotations forced by the change of the external magnetic field. The blocking temperature is much lower than that observed for the matrix free bulk compound as shown in III-A-1, while the residual magnetic moment at 0 Oe is much larger than the bulk material.

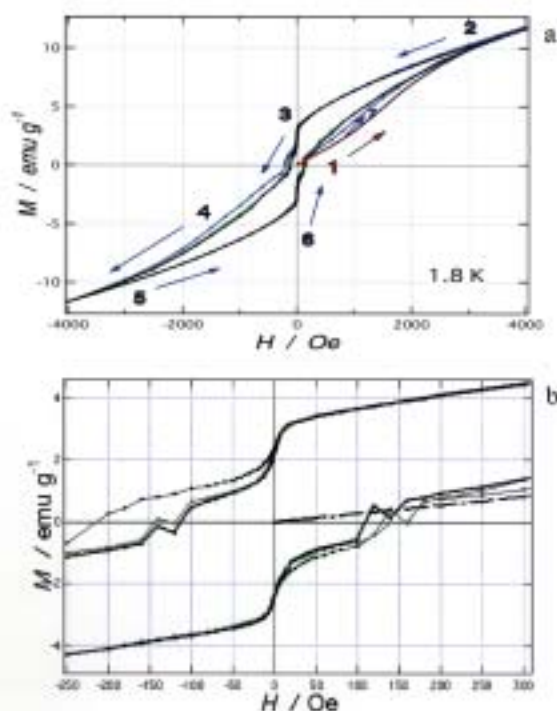


Figure 1. a: Magnetic moment hysteresis observed for $\text{Co}_x(\text{CH})_y(\text{CH}_2)_z$ magnets in a matrix composed of $(\text{C}_5\text{H}_5)\text{Co}(\text{C}_5\text{H}_5)$ and its derivatives. Note that the initial magnetization curve is located lower than that the second magnetization loop. b: Expanded view around low magnetic field.

III-A-3 Photochemical Generation of High Spin Clusters in Solution: (Cyclopentadienyl-Vanadium)_mO_n

HINO, Kazuyuki¹; INOKUCHI, Yoshiya; KOSUGI, Kentaroh; SEKIYA, Hiroshi¹; HOSOKOSHI, Yuko;

INOUE, Katsuya; NISHI, Nobuyuki
(¹Kyushu Univ.)

Organometallic clusters containing oxygen atoms, $(\text{CpV})_m\text{O}_n$ ($\text{Cp} = \text{C}_5\text{H}_5$), are generated by photochemical reaction of $\text{CpV}(\text{CO})_4$ in CH_2Cl_2 solution under control of oxygen contents. Mass spectra of single batch reactions exhibit strong signals assigned to low mass oxide clusters; $(\text{CpV})_4\text{O}_4$, $(\text{CpV})_5\text{O}_6$, and $(\text{CpV})_6\text{O}_n$ ($n = 6\sim 8$). Successive addition of reactant solution into the

photochemical reaction vessel shows the addition of $(\text{CpV})_m$ to the low mass oxide clusters producing $(\text{CpV})_m\text{O}_n$ ($m \gg n = 4\sim 7$). The magnetic susceptibility (χ_g) of the mixture of the former low mass products shows antiferromagnetic behavior, while that of the latter high mass products is as high as $4.6 \times 10^{-4} \text{ cm}^3 \text{ g}^{-1}$ at 10 K and the additional part due to high mass products behaves ferromagnetically at temperatures higher than 70 K.

III-B States of Neutral and Ionic Molecular Associates in Solutions

States of molecular associates particularly in aqueous solutions are of great importance in understanding the role of molecules in living organisms. We found that any ideally mixed state cannot be seen in protic-protic mixtures such as water-alcohol, water-acetic acid, and alcohol-acetic acid systems on the molecular level at solute molar fractions (χ_A) higher than 0.001. In such a system, solute-solute association is highly favored resulting in microscopic phase separation. Here we demonstrate that aprotic solvent such as acetonitrile can produce ideally mixed state(s) for acetic acid.

III-B-1 States of Molecular Associates in Binary Mixtures of Acetic Acid with Aprotic Polar Solvents: the Nature of Mixture States at Molecular Levels

NAKABAYASHI, Takakazu; NISHI, Nobuyuki

The structures and dynamics of liquids have received much attention over the past three decades. Our recent studies of Raman spectroscopy have shown that binary solutions of acetic acid with protic solvents do not get ideally mixed on the molecular level at acetic acid molar fractions (χ_A) higher than 0.001. In aprotic polar solvents, however, the C=O stretching band of acetic acid shows the mixing ratio dependence different from that in protic solvents. Temperature dependence of the Raman spectra of the acetic acid and acetonitrile binary solution at $\chi_A = 0.01$ is shown in Figure 1. As the temperature grows, the 1725 cm^{-1} band shifts to a lower-wavenumber, while the 1754 cm^{-1} band shifts to a higher-wavenumber. The intensity of the 1754 cm^{-1} band relative to that of the 1725 cm^{-1} band becomes larger with increasing temperature. The relative intensity between the two bands is independent of the acid concentration. These results suggest that the two bands arise from two types of acetic acid monomers in different environment. To examine the two different types of acetic acid monomers in acetonitrile, ab initio calculations are carried out with self-consistent reaction field method (B3LYP/6311++G** level). The dipole moment of a dipolar molecule becomes larger on going from the gas phase to the acetonitrile solution. Thus the C=O bond of the acetic acid monomer becomes longer and its C=O stretching mode shifts to a lower-wavenumber in acetonitrile. However, the C=O mode of the cyclic dimer in Figure 1 shows a higher-wavenumber shift in acetonitrile, because of the

decrease in the C=O...H-C interaction. These results indicate that the C=O band of the cyclic dimer shifts to a lower-wavenumber and that of the non-complexed acetic acid monomer shifts to a higher-wavenumber as the solute-solvent electrostatic interaction decreases. The dielectric constant decreases with increasing temperature, which means that the electrostatic interaction becomes weaker as the temperature grows. Thus, the positional changes in Figure 1 can be explained when the 1725 and 1754 cm^{-1} bands are assigned to the cyclic dimer and the non-complexed acetic acid monomer, respectively. Such two bands are also observed in other aprotic polar solvents such as 1,4-dioxane, indicating that the two types of acetic acid monomers are also exist in other aprotic polar solvents. It is therefore concluded that acetic acid molecules preferentially exist as the monomeric forms in the aprotic polar solvents. This means that ideally-mixed states at molecular levels exist in the binary solutions of acetic acid and the aprotic polar solvents when the mole fraction of acetic acid is small. From several spectroscopic studies on other binary solutions, the mixing rules at molecular levels may be proposed as follows: protic-protic binary mixtures do not easily become ideally-mixed states even when the mixing ratio is large, while ideally-mixed states at molecular levels appear in protic-protic binary mixtures at low concentrations of the protic solvent.

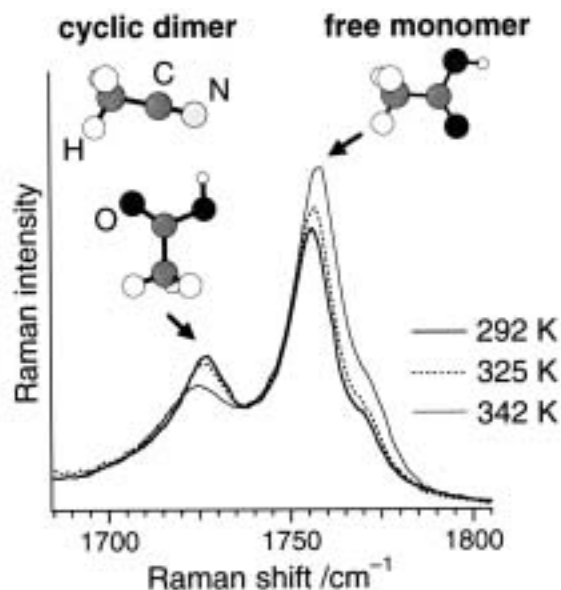


Figure 1. Temperature dependence of the C=O bands of the acetic acid and acetonitrile mixture.

III-B-2 Structure of Clusters in Methanol-Water Binary Solutions Studied by Mass Spectrometry and X-Ray Diffraction

TAKAMUKU, Toshiyuki¹; YAMAGUCHI, Toshio²;

ASATO, Masaki³; MATSUMOTO, Masaki³; NISHI, Nobuyuki

(Saga Univ.¹; Fukuoka Univ.²; Kyushu Univ.³)

[Z. Naturforsch., A: Phys. Sci. 55, 513 (2000)]

The structure of clusters in methanol-water solutions in its dependence on the methanol mole fraction χ_M has been investigated by mass spectrometry on clusters isolated from submicron droplets by adiabatic expansion in vacuum and by X-ray diffraction on the bulk binary solutions. The mass spectra have shown that the average hydration number, (n_m), of m -mer methanol clusters decreases with increasing χ_M , accompanied by two inflection points at $\chi_M = \sim 0.3$ and ~ 0.7 . The X-ray diffraction data have revealed a similar change in the number of hydrogen bonds per water and/or methanol oxygen atom at ~ 2.8 Å. On the basis of both results, most likely models of clusters formed in the binary solutions are proposed: at $0 < \chi_M < 0.3$ tetrahedral-like water clusters is the main species, at $0.3 < \chi_M < 0.7$ chain clusters of methanol molecules gradually evolve with increasing methanol content, and finery at $\chi_M > 0.7$ the chain clusters of methanol molecules become predominant. The present results are compared with clusters previously found in ethanol-water binary solutions and discussed in relation to anomalies of the heat of mixing of methanol-water binary solutions.

III-C Ultrafast Dynamics and Structural Changes of Aromatic Cation Radicals

Release of an electron from a neutral molecule by photons induces eminent structural changes of the molecule and reorientation of solvent molecules. In particular, polar solvents stabilize the newly born cation due to Coulombic interaction causing thermal excitation of surrounding solvents and the cation. Geminate recombination of the ejected electrons and the parent cations is also expected. We have studied the ultrafast dynamics upon photoionization of aromatic molecules by time-resolved absorption and Raman spectroscopic techniques.

III-C-1 Ultrafast Relaxation Dynamics of Aromatic Cation Radicals Following Photoionization

NAKABAYASHI, Takakazu; KAMO, Satoshi¹; SAKURAGI, Hirochika¹; NISHI, Nobuyuki
(¹Univ. Tsukuba and IMS)

Photoionization in condensed phases has been a subject of interest for many years. Charge-pair generation, recombination, solvation and vibrational relaxation processes as well as cation structural changes can occur after photoionization of aromatic molecules in solvents. In the previous study, solvation and vibrational relaxation processes occurring on a picosecond time scale are discussed.¹⁾ In the present study, we have measured femtosecond time-resolved absorption spectra of aromatic cation radicals (naphthalene, biphenyl, and 1,4-diphenylbutadiene) in nonpolar and polar solvents and discussed the dynamics of the photoionization in the

subpico- to picosecond time range. Figure 1 shows the time-resolved absorption spectra of the cation radical of naphthalene in cyclohexane. The broad absorption decays in several picoseconds, which can be attributable to the geminate recombination of the electrons with their parent cation radicals. The induced absorption in acetonitrile, however, shows the temporal profile different from that in cyclohexane. As shown in Figure 2, the absorption intensity first decreases in the subpicosecond range, and then increases on a 10–20 ps time scale. The absorption around 700 nm also shifts to a lower-wavelength with the delay time. The picosecond increase in the absorption intensity is observed in all the region of 600–740 nm. The temporal profile observed in ethyl acetate is similar to that in acetonitrile. The subpicosecond decay components can be ascribed to the geminate recombination of the unsolvated cation radical, which competes with the reorganization of solvent molecules. To our best knowledge, it is the first report to observe the ultrafast geminate recombination

of unsolvated aromatic cation radicals in polar solvents. The picosecond increase in the absorption intensity is observed in all the cation radicals treated, suggesting that the picosecond relaxation process increasing the cation absorption intensity occurs after the photoionization of the aromatic molecules. The time scale of the change in the absorption intensity is the same as that of the vibrational relaxation, while the intensity rise does not correlate with the dielectric relaxation time. The picosecond rise is significantly observed in highly polar solvents forming strong solvent-solute interactions. From these observations, we propose the model that the thermal excitation of the solvent shell disturbs the solvation structure of the cation radical, which causes the change in the cation absorption intensity. Contrary to the generally accepted view, this result suggests that the cation radical formed by the multi-photon ionization is solvated on a 10–20 ps time scale, because of the thermal excitation of the neighboring solvent shell.

Reference

- 1) T. Nakabayashi, S. Kamo, H. Sakuragi and N. Nishi, *J. Phys. Chem. A* in press.

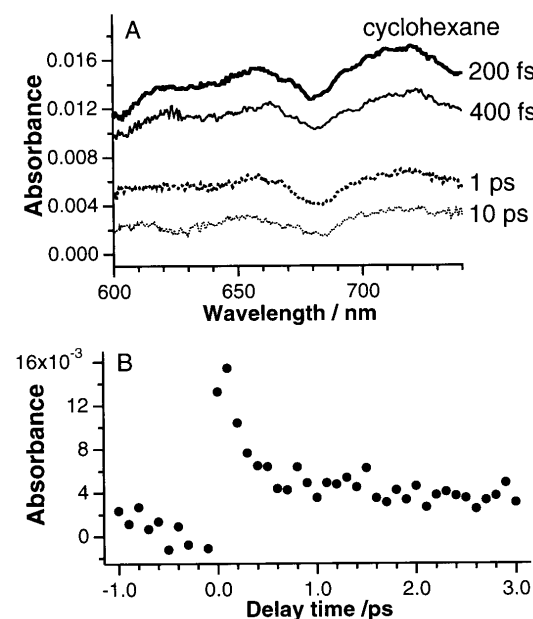


Figure 1. (A) Femtosecond time-resolved absorption spectra of naphthalene cation radical in cyclohexane. (B) Temporal profile of the absorbance due to naphthalene cation radical in cyclohexane at 685 nm.

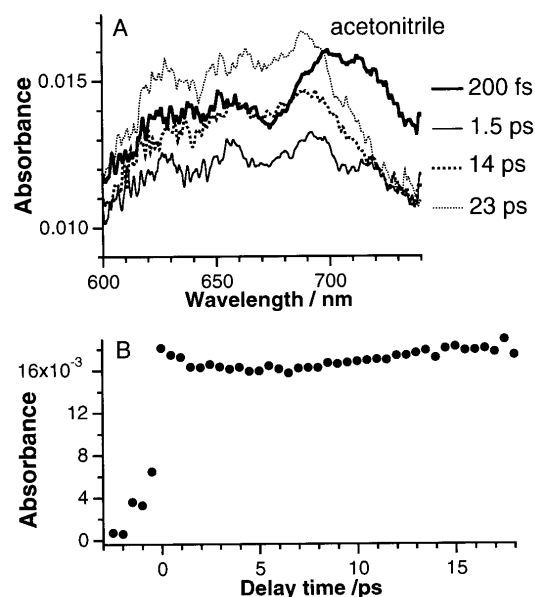


Figure 2. (A) Femtosecond time-resolved absorption spectra of naphthalene cation radical in acetonitrile. (B) Temporal profile of the absorbance due to naphthalene cation radical in acetonitrile at 685 nm.

III-D Spectroscopic and Dynamical Studies on Charge Delocalization and Charge Transfer in Molecular Cluster Ions

Electron deficiency of molecular cluster cations can attract electron rich groups or atoms exhibiting a charge transfer or a charge resonance interaction in the clusters. These interactions cause dynamical changes of structures such as proton transfer or ion-core switching in hot cluster ions.

III-D-1 Photodissociation Spectroscopy of Benzene Cluster Ions in Ultraviolet and Infrared Regions. Static and Dynamic Behavior of Positive Charge in Cluster Ions

INOKUCHI, Yoshiya; NISHI, Nobuyuki

[*J. Chem. Phys.* **114**, 7059 (2001)]

Photodissociation spectroscopy is applied to benzene cluster ions in ultraviolet and infrared regions. In the ultraviolet photodissociation spectrum of $(C_6H_6)_3^+$, a characteristic broad band emerges at 255 nm. This band is assigned to a $\pi^* \leftarrow \pi$ transition of a solvent benzene molecule that exists in the trimer. This is in accord with a previous model of the ion cluster with a dimer ion core and a solvent benzene molecule. Infrared photodissociation spectra of $(C_6H_6)_n^+$ ($n = 3-5$) show a sharp band at 3066 cm^{-1} . The band is attributed to a C–H stretching vibration of the dimer ion core. The infrared spectra of $(C_6H_6)_n^+$ ($n = 3-5$) are fitted to model spectra produced by combining the C–H stretching bands of the dimer ion core and the solvent benzene molecule. Infrared photodissociation spectra of mixed benzene trimer ions with one or two benzene- d_6 molecules demonstrate that there is no correlation between the excited dimer ion core site in the trimer and the photofragment dimer ion species. This result implies that a dimer ion core switching occurs in photoexcited vibrational states prior to the dissociation.

III-D-2 Infrared Photodissociation Spectroscopy of Protonated Formic Acid-Water Binary Clusters, $H^+(HCOOH)_n \cdot H_2O$ ($n = 1-5$). Spectroscopic Evidence of Ion Core Switch Model

INOKUCHI, Yoshiya; NISHI, Nobuyuki

Static and dynamic features of the positive charge distribution in cluster ions are very important, because they are related very much with the charge transportation in condensed phases. In this study, we apply infrared (IR) photodissociation spectroscopy to protonated formic acid-water binary clusters, $H^+(HCOOH)_n \cdot H_2O$ ($n = 1-5$). We also investigate ab initio molecular orbital calculations to obtain optimized structures and theoretical IR spectra. By comparing the observed IR photodissociation spectra with the calculated ones, we discuss structures and an ion core switching process in these clusters.

The IR photodissociation spectra of $H^+(HCOOH)_n \cdot H_2O$ ($n = 1-5$) are measured by using an ion guide spectrometer with two quadrupole mass filters. The MO calculations are performed by using the Gaussian 98 program package at B3LYP/6-31G(d,p) level.

Figure 1 shows the IR photodissociation spectra in the $3100-3800\text{ cm}^{-1}$ region. For $n = 1-3$, there are two maxima in the IR spectra. We assign the low-frequency bands to free OH stretching vibrations of the formic acid molecules. The high-frequency bands are ascribed to asymmetric OH stretching vibrations of the water molecules. For $n = 4$, the high-frequency band disappears from the spectrum. For $n = 5$, no sharp bands exist in the spectrum. Because the free OH stretching band of water (the high-frequency band) is not observed for $n = 4$ and 5, the H_2O molecule is in the periphery of the clusters for $n \leq 3$, but it is located in an inner position of the clusters for $n > 3$. Furthermore, the theoretical calculations predict that the ion-core switch occurs from $HCOOH_2^+$ to H_3O^+ between $n = 3$ and 4. The most stable structures of $n = 4$ and 5 predicted by the theoretical calculations are also shown in Figure 1.

In the clusters of $n = 4$ and 5, the ion core is H_3O^+ . The H_3O^+ ion core is thought to be unstable due to the lower proton affinity of water (165 kcal/mol) than that of formic acid (177.3 kcal/mol). However, the formic acid molecules surround and stabilize the H_3O^+ ion cores in the clusters. In summary, the ion core switch really occurs from $HCOOH_2^+$ to H_3O^+ between $n = 3$ and 4 in $H^+(HCOOH)_n \cdot H_2O$.

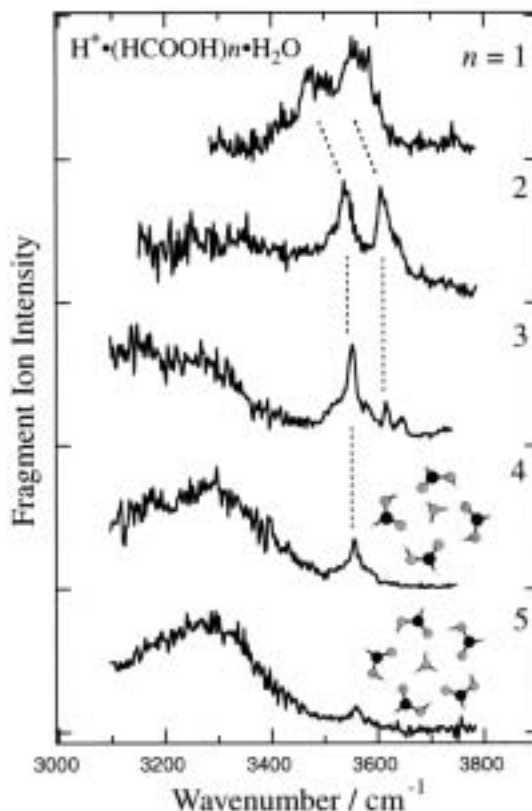


Figure 1.

III-D-3 Charge Transfer Interaction in Acetic Acid-Benzene Cation Complex

KOSUGI, Kentaroh; INOKUCHI, Yoshiya; NISHI, Nobuyuki

[*J. Chem. Phys.* **114**, 4805 (2001)]

Geometrical and electronic structures of acetic acid-benzene cation complex, $(CH_3COOH) \cdot (C_6H_6)^+$, are studied experimentally and theoretically. Experimentally, a vibrational spectrum of $(CH_3COOH) \cdot (C_6H_6)^+$ in the supersonic jet is measured in the $3000-3680\text{ cm}^{-1}$ region using an ion-trap photodissociation spectrometer. An electronic spectrum is also observed with this spectrometer in the $12000-29600\text{ cm}^{-1}$ region. Theoretically, ab initio molecular orbital calculations are performed for geometry optimization and evaluation of vibrational frequencies and electronic transition energies. The frequency of the strong band (3577 cm^{-1}) is close to that of the O–H stretching vibration of acetic acid and the weak one is located at 3617 cm^{-1} . On the basis of geometry optimizations and frequency calculations, the strong band is assigned to the O–H stretching vibration of the *cis*-isomer of acetic acid in

the hydrogen-bonded complex (horizontal *cis*-isomer). The weak one is assigned to the vertical *trans*-isomer where the *trans*-isomer of acetic acid interacts with the π -electron system of the benzene cation. The weakness of the high frequency band in the photodissociation spectrum is attributed to the binding energy larger than the photon energy injected. Only hot vertical *trans*-isomers can be dissociated by the IR excitation. The electronic spectrum exhibits two bands with intensity maxima at 17500 cm^{-1} and 24500 cm^{-1} . The calculations of electronic excitation energies and oscillator strengths suggest that charge transfer bands of the vertical *trans*-isomer can be observed in this region in addition to a local excitation band of the horizontal *cis*-isomer. We assign the 17500 cm^{-1} band to the charge transfer transition of the vertical *trans*-isomer and the 24500 cm^{-1} band to the π - π transition of the horizontal *cis*-isomer. The calculations also suggest that the charge transfer is induced through the intermolecular $\text{C}\cdots\text{O}=\text{C}$ bond formed between a carbon atom of benzene and the carbonyl oxygen atom of acetic acid.